Key melt properties for controlled synthesis of glass beads by aerodynamic levitation coupled to laser heating

Jan Baborák, Maureen Yembele, Petr Vařák, Sandra Ory, Emmanuel Véron, Michael J Pitcher, Mathieu Allix, Pavla Nekvindová, Alessio Zandonà

Key melt properties for controlled synthesis of glass beads by aerodynamic levitation coupled to laser heating

Jan Baborák[1,2], Maureen Yembele[2,3], Petr Vařák[1], Sandra Ory[2], Emmanuel Véron[2], Michael J. Pitcher[2], Mathieu Allix[2], Pavla Nekvindová[1], Alessio Zandonà[2,4]*

[1] Department of Inorganic Chemistry, University of Chemistry and Technology, Technická 5, 166 28, Prague, Czech Republic
[2] CNRS, CEMHTI UPR3079, Univ. Orléans, F-45071 Orléans, France
[3] Laboratoire commun Canopée, CNRS, Univ. Lorraine, Saint Gobain, France
[4] Friedrich-Alexander-Universität Erlangen-Nürnberg, Department of Materials Science (Glass and Ceramics), Martensstr. 5, 91058 Erlangen, Germany

Abstract

Binary alkali silicate glasses were synthesized as beads by aerodynamic levitation coupled to laser heating to test the applicability of the method to this compositional range. While bubble-free lithium disilicate beads could be easily obtained, sodium and potassium silicates proved more challenging to melt without significant alkali evaporation: the final samples contained bubbles and exhibited compositional drifts compared to the starting stoichiometry, especially at high SiO_2 content. The risk of volatilization from the melts was evaluated empirically: the volatility of each oxide component scaled to the ratio between its melting temperature T_m and the T_m of the target composition (r_{evap}), while the difference between such ratios (Δ_{evap}) provided a qualitative estimation of the risk of differential evaporation. The formulated approach enables to evaluate the suitability of aerodynamic levitation synthesis for a given target glass composition: while low melting temperature and low liquidus viscosity ($\eta < 10^0$ Pa s) represent the primary optimal conditions, more viscous materials can still be prepared without major compositional drifts using a more careful melting procedure, especially if r_{evap} and Δ_{evap} are minimized.

Keywords: aerodynamic levitation coupled to laser heating (ADL), alkali silicate glass, glass beads, viscosity, high-temperature evaporation

***Corresponding author:** Alessio Zandonà, alessio.zandona@fau.de

1. Introduction

Thanks to unique properties such as viscous flow, glass-forming melts can be shaped in well-defined and complex geometries with good-quality surface finishes. These features are essential for the widespread cost-effective use of glass for the production of, for instance, hollow containers and flat window panes[1]. Depending on the desired final geometry, numerous shaping methods have been developed by the glass industry, from simple casting to glass blowing and float processing[2]. Specifically concerning the manufacturing of spherical glass beads, which have found historical applications in jewelry[3] and, more recently, as optical lenses and retro-reflective paint additives[4], several manufacturing routes have been reported (for instance[5–7]), which however exhibit only limited compositional versatility and size selectivity.

On the other hand, academic researchers in materials science and solid-state chemistry have been synthesizing glass beads for decades using aerodynamic levitation coupled to laser heating (ADL)[8, 9], in order to study the properties of melts at high temperature (e.g. by X-ray or neutron scattering)[10, 11] but also as a response to the evergrowing push towards new materials discovery[12]. Indeed, this containerless method facilitates the vitrification of compositions (e.g. aluminates[13–20], gallates[14, 21–24], titanates[25, 26], niobates[27, 28], tungstates[29]) which fall substantially outside the category of classically defined glass formers, due to the possibility of achieving very high melting temperatures (up to 3300 K) and fast cooling rates (~300 K s^{-1}), additionally suppressing heterogeneous crystal nucleation and avoiding potential sample-crucible reactions. These exotic compositions, both in their glassy state and after controlled crystallization, can exhibit interesting features (e.g. high refractive index and transparency, persistent luminescence, advantageous electrical and mechanical properties) which make them promising candidates for future technological applications.

Although numerous studies also reported the ADL synthesis and characterization of silicate or borate glasses and melts (for instance[30–47]), the strong volatility of some chemical components[48–50] (e.g. B_2O_3 and alkali oxides) under laser irradiation still represents a major drawback of ADL-driven materials discovery, limiting its applicability within these chemical domains. Borate and silicate glasses can be easily prepared by conventional melt-quenching, but ADL was recently shown to provide a superior approach to

elucidate transition metal saturation and homogenous nucleation in aluminosilicate glasses and glass-ceramics[51–53], again taking advantage of the high melting temperatures, fast cooling rates and suppression of heterogeneous surface nucleation. Furthermore, it can be speculated that the shaping capabilities of ADL may provide a cost-effective route to manufacture high-added-value optical components, especially considering the increasing need for miniaturized imaging systems in portable electronic devices[54].

Consequently, this study aims to assess key melt parameters such as glass-forming ability, melting point, viscosity and high-temperature evaporation tendency, to identify the optimal conditions for reproducible glass synthesis by ADL taking binary alkali silicates as model samples. The overall analysis is meant to facilitate an even unexperienced user in successfully approaching materials discovery and high-temperature melt characterization by ADL, evaluating beforehand the suitability of the target compositions and possibly minimizing the risks related to high-temperature volatilization.

2. Experimental

2.1 Glass synthesis

Binary silicate glasses were selected for this work to investigate the challenges of synthesizing glasses by ADL over a broad range of melt viscosities and evaporation tendencies, thereby focusing on simple compositions. In the following, the synthesis of nine compositions of glass by conventional melt-quenching and/or ADL is studied: three lithium silicates, i.e. **LS2** ($Li_2O{\cdot}2SiO_2$), **LS4** ($Li_2O{\cdot}4SiO_2$) and **LS8** ($Li_2O{\cdot}8SiO_2$); three sodium silicates, i.e. **NS2** ($Na_2O{\cdot}2SiO_2$), **NS4** ($Na_2O{\cdot}4SiO_2$) and **NS8** ($Na_2O{\cdot}8SiO_2$); three potassium silicates, i.e. **KS2** ($K_2O{\cdot}2SiO_2$), **KS4** ($K_2O{\cdot}4SiO_2$) and **KS8** ($K_2O{\cdot}8SiO_2$). Raw materials for the synthesis included: silicon oxide SiO_2 (Alfa Aesar, 99.5%), lithium carbonate Li_2CO_3 (Aldrich, 99%), sodium carbonate Na_2CO_3 (Strem chemicals, 99.5+%), potassium carbonate K_2CO_3 (Fluka, 99%). All glasses were stored in a desiccator to avoid reaction with H_2O and CO_2 from the air.

ADL was used to prepare beads of the listed nine compositions. To facilitate the analysis of the ADL method, 3 g of LS2, NS2 and KS2 were additionally synthesized as reference materials by conventional melt-quenching. The precursor carbonates and SiO_2 for each glass batch were suspended in

ethanol and mixed in an agate mortar; when the ethanol evaporated, the mixture was loaded into a small Pt crucible and heated up in an electric furnace with a rate of 10 K min^{-1} up to 1173 K. This temperature was held for 1 h to allow for full reaction of the powder precursors. Subsequently, the samples were heated at the same rate to 1623 K and melted for 1 h. Finally, the samples were extracted from the furnace and quenched by rapidly immersing the bottom of the Pt crucible in water. To ensure good homogeneity, the melting at 1623 K for 1 h was repeated after crushing each sample into fine powder. The obtained glass shards were transparent with no observable bubbles or heterogeneities.

The above-mentioned chemical precursors were used also to prepare samples by ADL on an experimental setup described in previous works[51, 52]. A novel procedure involving the addition of a binder (cornstarch) to a water-based slurry was tested and carefully optimized to quickly prepare numerous well-compacted hemispherical pellets of very reproducible mass (35±5 mg). Their shape enabled stable levitation and the achievement of containerless conditions from the beginning of the synthesis; the well-defined starting mass favored a strict control over the synthesis parameters (e.g. cooling rate), while their improved mechanical stability minimized material loss due to pellet breakage and supported the subsequent evaluation of mass losses solely due to evaporation. 2 g of precursors were mixed with cornstarch (5% in mass of the inorganic powders) and water until obtaining a slurry of suitable viscosity. A syringe was then used to deposit small drops of this slurry on an aluminum foil, where they were left overnight to dry at room temperature into hemispherical greens; drying was completed in an electric furnace for 2 h at 473 K to ensure full compaction (note that cornstarch decomposes at approximately 600 K[55]). Pellets prepared this way were then placed into the ADL copper nozzle, levitated by a stream of oxygen and melted using two CO_2 (10.6 μm) lasers with a heating protocol of ~45 s in total (Fig. 1). Gas flow rate and gas composition were previously shown to have a strong impact on volatilization[56] and were therefore kept constant throughout the experiments to focus solely on differences arising from the composition of the samples. The melting process was monitored with the help of a camera, while the temperature was estimated with a pyrometer (wavelength = 0.9 μm). In the absence of an accurate emissivity calibration for each sample,

temperature readings may vary by as much as ±100 K at the maximum laser power but still allow a consistent approach across different compositions.

The expected increasing temperature sensitivity (i.e. tendency towards high-temperature vaporization[48–50]) of the samples along the series LS*X*-NS*X*-KS*X* (*X* = 2, 4 or 8) was tackled using the following synthesis strategy: LS*X* samples were invariably prepared first, optimizing the melting parameters (temperature reading, time) to minimize their high-temperature dwell while still obtaining good-quality glass beads with (possibly) no bubbles visible to the naked eye. Then, the exact same procedure was applied to the corresponding NS*X* and KS*X* samples, as visualized on Fig. 1; note that the same temperature readings as for LS*X* could be achieved for NS*X* and KS*X* samples using an equal or lower laser power, supporting the reliability of the results concerning high-temperature evaporation (see below). More specifically, we performed the syntheses at maximum pyrometer readings of ~1500 °C for *M*S2, ~1700 °C for *M*S4 and ~1800 °C for *M*S8. Samples prepared in this way were glassy and transparent, with a variable bubble content.

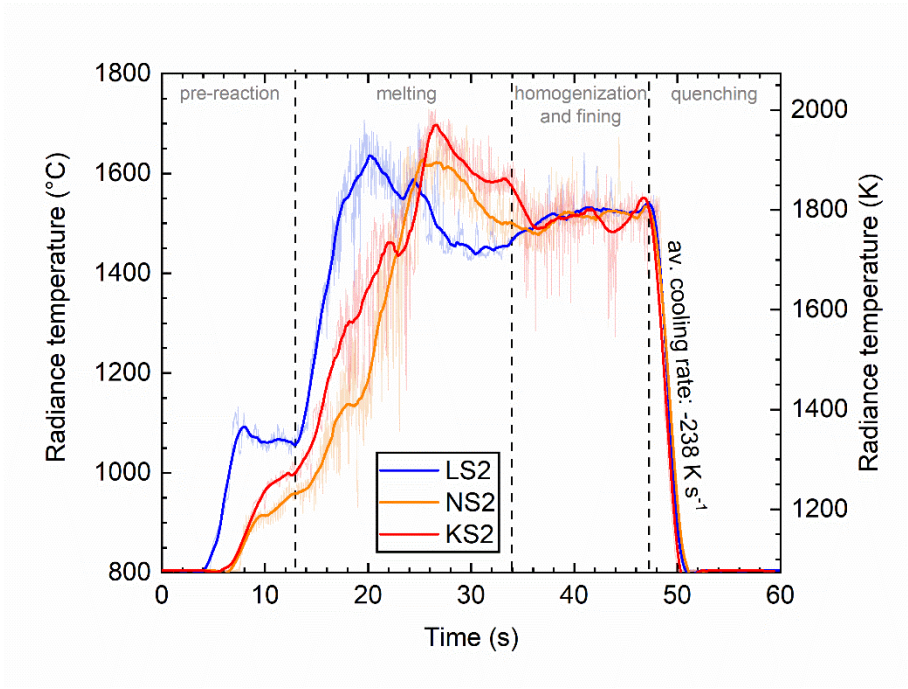

Figure 1. Example of time-temperature curves acquired with a 0.9 µm pyrometer during ADL synthesis of LS2, NS2 and KS2 glass beads, schematically separated into four main stages: pre-reaction, melting,

temperature homogenization and fining, quenching. The pyrometer reading (light color shades) is noisy due to instabilities during the levitation. The signal was smoothed (thick curves) using a Savitzky-Golay filter[57] (second polynomial order). The rate of the free cooling was estimated between the beginning of the quench (1801 K at 47 s) and the end of signal detection (1070 K at 50 s).

In order to test the validity of our approach over a wider compositional range, we melted two additional samples according to the same procedure: a lithium borate LB2 ($Li_2O{\cdot}2B_2O_3$) using Li_2CO_3 (Aldrich, 99%) and H_3BO_3 (Alfa Aesar, 99.5%) precursors and a sodium phosphate NP ($Na_2O{\cdot}P_2O_5$) using NaH_2PO_4 (Aldrich, 99%) as a precursor. In both cases, glass beads could be easily obtained without any signs of evaporation loss, at maximal pyrometer readings of 1050 °C and 1125 °C respectively. Sample LB2 was subsequently intentionally heated to higher temperatures (up to 1200 °C) to induce high-temperature volatilization and mass loss.

2.2 Glass characterization

The three compositions synthesized by conventional melt-quenching (LS2, NS2 and KS2) were characterized by differential scanning calorimetry (DSC) to investigate their glass stability and glass transition temperature T_g, using a SETARAM Multi HTC 1600 and loading ~500 mg of powder in the Pt crucibles for each measurement. First, simple upscans were performed up to 1173 K and used to estimate glass stability according to the Hrubý method[58]:

$$K_{gl} = \frac{T_c - T_g}{T_m - T_c} \qquad \text{(Eq. 1)}$$

where T_c stands for the crystallization onset, T_g for the glass transition temperature and T_m for the melting temperature. The real T_g of the samples (viscosity $\eta \approx 10^{12}$ Pa s) was obtained by rate-matching measurements at 10 K min^{-1}: the glass samples were heated beyond their glass transition to achieve melt relaxation, subsequently cooled at 10 K min^{-1} to constraint their thermal history and then measured during a second upscan at 10 K min^{-1}. During this segment, the glass transition onset (T_{onset}) was extracted from

the heat flow curve using the double-tangent method. As demonstrated in previous works[59–63], rate-matching DSC measurements can be associated to viscosity η through the relation:

$$log_{10}\eta(T_{onset}) = -log_{10}|q_{c,h}| + K_{onset} \quad \text{(Eq. 2)}$$

where $q_{c,h}$ is the heating and cooling rate applied during DSC measurements and K_{onset} is a constant, calibrated at 11.20(±0.15) Pa s. For $q_{c,h}$ = 10 K min^{-1}, one obtains $\log_{10}\eta(T_{onset})$ = 11.98 Pa s ≈ 12 Pa s.

Based on T_g values obtained from DSC and data from the literature[61, 64], full viscosity curves were fitted for the three compositions LS2, NS2 and KS2, using the Waterton-Mauro-Yue-Ellison-Gupta-Allan (w-MYEGA) equation[65, 66]:

$$log_{10}\eta = log_{10}\eta_\infty + (12 - log_{10}\eta_\infty)\frac{T_g}{T} exp\left[\left(\frac{m}{12 - log_{10}\eta_\infty} - 1\right)\left(\frac{T_g}{T} - 1\right)\right] \quad \text{(Eq. 3)}$$

in which $\log_{10}\eta_\infty$ defines viscosity at the limit of infinite temperature and m the melt fragility. For the fits, only these two parameters were varied, while T_g was fixed to the values obtained from DSC.

Concerning ADL synthesis, high-temperature evaporation was monitored by measuring the mass of each dried pellet (still including only the inorganic precursors and the cornstarch, assuming all H_2O was lost during drying at 200 °C) and of the respective resulting glass bead; the mass of the pellets allowed to calculate the expected bead mass (after subtracting the mass of the corn starch and of CO_2 removed during melting) and compare it to the measured one, estimating mass losses due to high-temperature evaporation. For each composition, ten pellets/beads were considered for statistics. One bead of each composition was then analyzed by Laser Ablation Inductively Coupled Plasma Mass Spectrometry (LA-ICP-MS) by adapting the analytical protocol developed at the IRAMAT-CEB for glass matrices[67]. On average, the beads had a diameter of 2 mm and were polished to study a cross section of the core of the bead. The laser ablated circular spots with a diameter of 0.1 mm; 4 acquisitions were performed (1 in the center and 3 near the edges) to confirm sample homogeneity and quantify compositional drifts due to evaporation. Due to their expected higher hygroscopicity, LB2 and NP beads were measured without any polishing step, shortly after the synthesis; two subsequent ablations at the same spot were used to confirm the homogeneity of the beads between surface region and interior.

3. Results

To measure some key properties and support the subsequent discussion of ADL processing, glasses LS2, NS2 and KS2 were first synthesized by conventional melt-quenching. Simple DSC upscans performed at 10 K min^{-1} on these samples revealed clear and expectable differences in glass stability, quantified through the Hrubý parameter K_{gl} [58] (**Tab. 1**): the temperature difference between glass transition and crystallization (and therefore similarly K_{gl}) increased substantially going from LS2 to NS2 and KS2 (**Fig. 2- a**). Based on the results of previous authors[68], we assumed that this higher glass stability also corresponds to a higher glass-forming ability of the respective melts.

T_g values (at which viscosity $\eta = 10^{11.98\pm0.15}$ Pa s) were obtained using rate-matching DSC measurements[59–63]: they enabled to fit full viscosity curves for the three glass-forming melts (**Fig. 2- b**), using high-temperature viscosity data from literature[61, 64]. While T_g increased going from LS2 to NS2 and KS2, fragility indices *m* exhibited an opposite trend (**Tab. 1**), eventually making KS2 the most viscous and LS2 the least viscous liquid among the three samples. At the melting temperature T_m, we calculated a viscosity of $10^{1.51}$ Pa s for LS2, $10^{2.94}$ Pa s for NS2 and $10^{2.38}$ Pa s for KS2.

Table 1. Parameters obtained from DSC measurements and viscosity fits of the reference samples synthesized by conventional melt-quenching: T_g stands for the glass transition temperature (from rate-matching DSC measurements at 10 K min^{-1}), T_c for the onset of crystallization (on simple DSC upscans at 10 K min^{-1}), T_m for the liquidus temperature (from literature[69–71]), K_{gl} for the glass stability parameter after Hrubý[58], *m* for the fragility index and $log_{10}\eta_\infty$ for the logarithmic viscosity at infinite temperature (from viscosity fits using the w-MYEGA model, Eq. 2). $log_{10}\eta(T_m)$ provides the viscosity at the melting temperature, calculated through the w-MYEGA fits.

Sample	Composition	T_g (K)	T_c (K)	T_m (K)	K_{gl}	m	$log_{10}\eta_\infty$ (η in Pa s)	$log_{10}\eta(T_m)$ (η in Pa s)
LS2	$Li_2O{\cdot}2SiO_2$	726±5	837±5	1306	0.24±0.02	41.4±0.7	-1.5±0.1	1.5
NS2	$Na_2O{\cdot}2SiO_2$	728±5	916±5	1148	0.81±0.03	37.1±0.9	-1.8±0.2	2.9
KS2	$K_2O{\cdot}2SiO_2$	768±5	1043±5	1309	1.03±0.03	34.6±0.9	-2.2±0.3	2.4

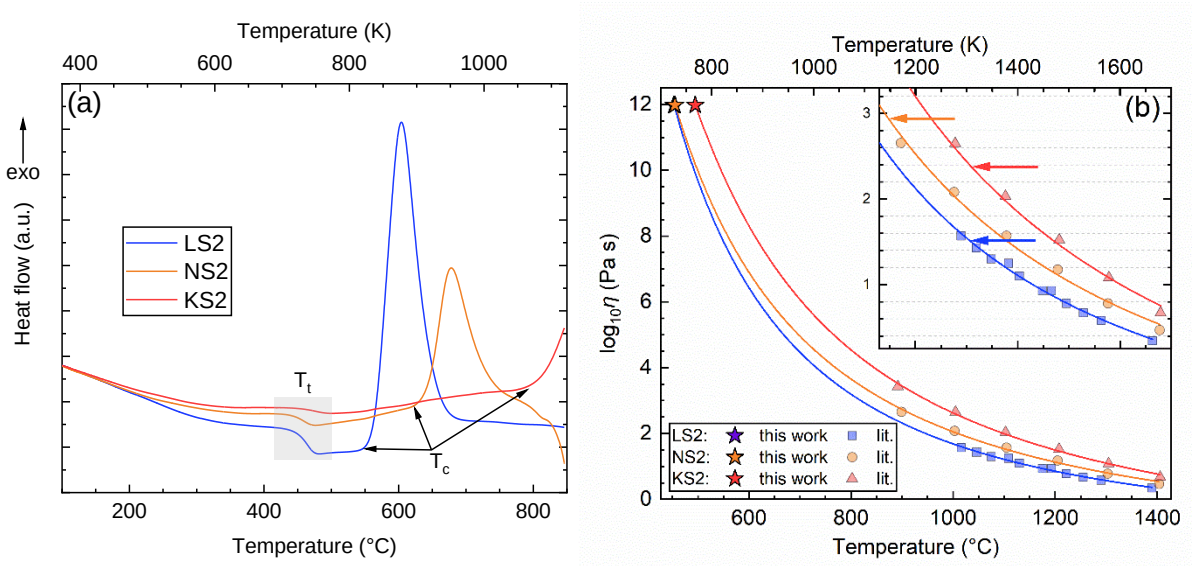

Figure 2. a) Heat flow curves obtained during DSC upscans at 10 K min^{-1} applied to samples LS2, NS2 and KS2 synthesized by conventional melt-quenching; a shaded area labeled as T_t marks the glass transition region, while T_c labels the onset of crystallization. b) w-MYEGA fits (fit parameters in **Table 1**) of the full viscosity curves of LS2, NS2 and KS2, based on the T_g values determined within this work and high-temperature viscosity data from literature[61, 64]. Horizontal arrows signal the viscosity at T_m for each composition.

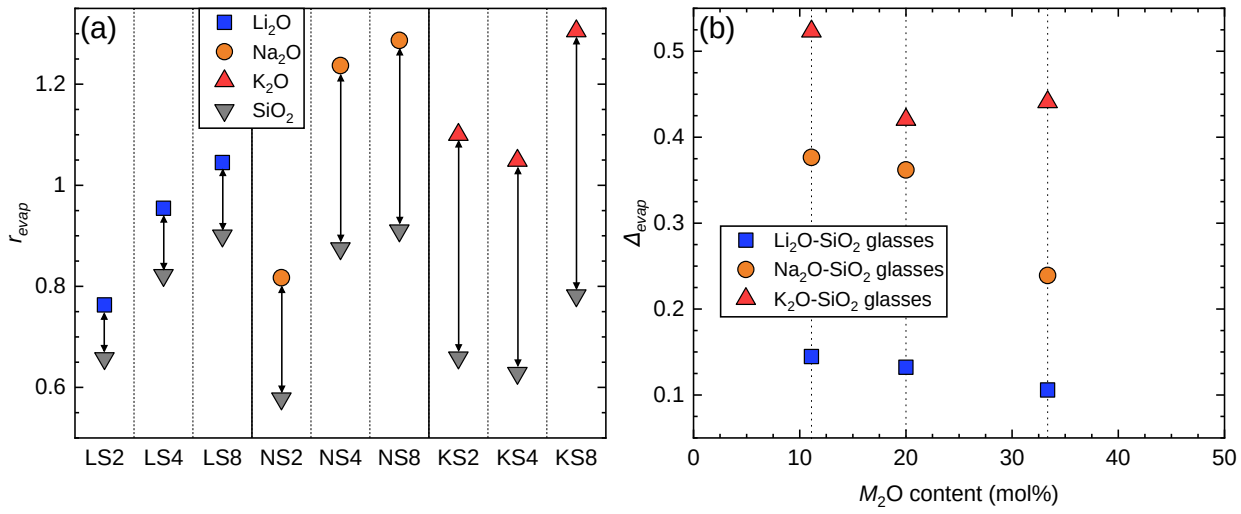

Figure 3. (a) r_{evap} (Eq. 4) and (b) Δ_{evap} (Eq. 5) parameters computed for the compositions analyzed within this work, using data from literature[69–71]. Vertical arrows in the (a) panel correspond to the Δ_{evap} values plotted in (b).

To obtain a crude prediction of the tendency towards high-temperature volatilization of the nine samples to be synthesized by ADL (LS2, LS4, LS8, NS2, NS4, NS8, KS2, KS4 and KS8), the two parameters r_{evap} (Eq. 4) and Δ_{evap} (Eq. 5) are here defined as:

$$r_{evap} = \frac{T_{m,\Sigma}}{T_m} \qquad \text{(Eq. 4)}$$

$$\Delta_{evap} = r_{evap,max} - r_{evap,min} \qquad \text{(Eq. 5)}$$

where T_m is the melting point of a given oxide component and $T_{m,\Sigma}$ the melting point of the target multicomponent glass (both obtainable from phase diagrams, see Table 2); $r_{evap,max}$ and $r_{evap,min}$ respectively stand for the highest and lowest r_{evap} values among all components of the target glass. As demonstrated below, a higher r_{evap} indicates an increasing tendency of a given oxide component to evaporate from the

respective multicomponent melt at high temperature. Especially if one of the melt components exhibits $r_{evap} > 0.8$ (indicative threshold based on the results of this work), Δ_{evap} can then be used to estimate the risk of evaporation-driven compositional drifts: increasing Δ_{evap} manifest an increasing risk of uneven high-temperature losses. The values for the melts analyzed within this work are summarized in Fig. 3: r_{evap} was observed to generally increase with a higher SiO_2 content in these binary glasses, due to the rising T_m of the mixtures. Alkali oxides invariably exhibited higher values as compared to SiO_2, with Li_2O plotting between 0.7 and 1.1, Na_2O between 0.8 and 1.3 and K_2O between 1.0 and 1.3. The observed trends mirrored those expectable based on previous literature sources analyzing the high-temperature vaporization of simple oxides[48–50]. Also, Δ_{evap} slightly increased proportionally to the SiO_2 content of the glasses, reaching the highest values in K_2O-containing samples (up to ~0.5) and the lowest in those containing Li_2O (~0.1).

Table 2. Melting points T_m from literature[69–71] and resulting r_{evap} and Δ_{evap} parameters for the nine samples analyzed within this work.

Sample	T_m	r_{evap}		Δ_{evap}
	(K)	M_2O	SiO_2	
LS2	1306	0.76	0.66	0.11
LS4	1633	0.95	0.82	0.13
LS8	1788	1.04	0.90	0.14
NS2	1148	0.82	0.58	0.24
NS4	1738	1.24	0.88	0.36
NS8	1808	1.29	0.91	0.38
KS2	1309	1.10	0.66	0.44
KS4	1248	1.05	0.63	0.42
KS8	1553	1.31	0.78	0.52

After this preliminary examination, ADL was used to synthesize glass beads of these nine target compositions. Due to the increasing melt viscosity inferred above, obtaining perfect bubble-free beads proved increasingly difficult moving from Li_2O- to Na_2O- and K_2O-bearing melts, as already inferable from a visual inspection of the samples (Fig. 4); a similar effect was noticed in the case of increasing SiO_2 content (e.g. in the series LS2-LS4-LS8). Despite the complexity of these phenomena, previous experiments performed both in a space laboratory and in normal gravity conditions suggest that the rotation of the droplet renders bubble escape even more challenging than in conventional melting, favoring bubble migration towards an axial position, with buoyancy playing a lesser role[72–74]. Bubbles are expected to originate from the decomposition of cornstarch and carbonate precursors, as well as from direct injection of the levitation gas jet during the initial melting stage, when the droplet has not yet achieved a stable spherical shape.

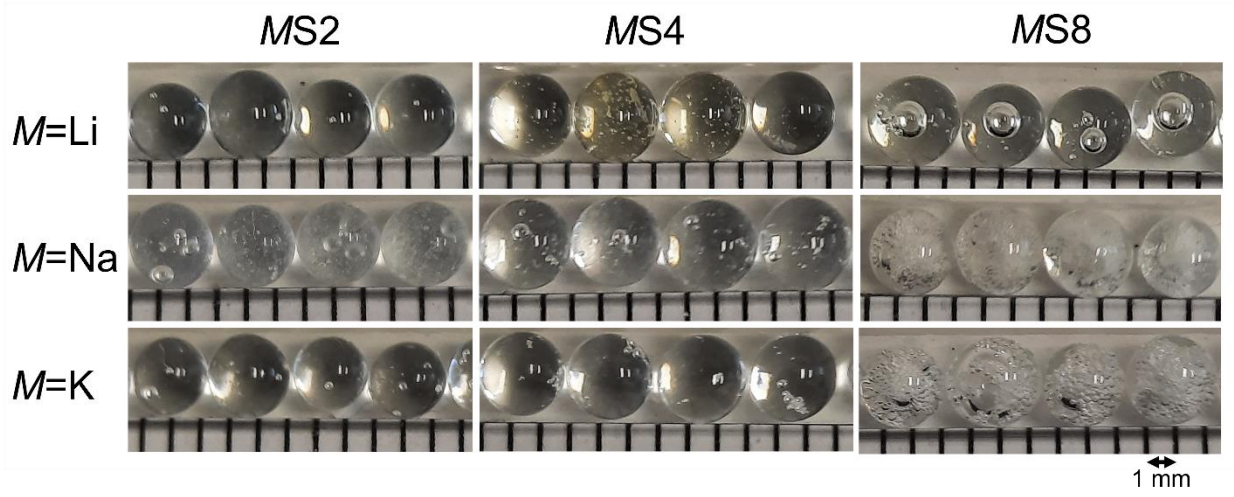

Figure 4. Pictures of beads synthesized by ADL. Visible influence of silica content and different alkali oxides. The distance between the vertical black bars is 1 mm.

The bead mass expected after decarbonation of the pellets and that of the synthesized glass beads was compared to quantify losses due to evaporation during ADL melting (Fig. 5-a); error bars on the graph are plotted according to the standard deviation of the data over ten measured beads. Note that the samples with lower content of silica were melted at lower temperatures (1800 K), while a higher melting temperature

(up to 2100 K) was required to prepare samples with lower M_2O content. Li_2O-bearing samples invariably plotted closer to the expected mass, while Na_2O- and especially K_2O-containing beads exhibited mass losses up to roughly 20%. In all cases, a lower initial content in alkali oxide (or alternatively a higher SiO_2 content) led to more noticeable mass losses. As demonstrated in Fig. 5-b, the average mass losses determined for the nine target compositions exhibited a clear correlation to the r_{evap} value of the most volatile components, i.e. the alkali oxides Li_2O, Na_2O or K_2O (as expectable from previous studies on the vaporization behavior of oxides[48–50]).

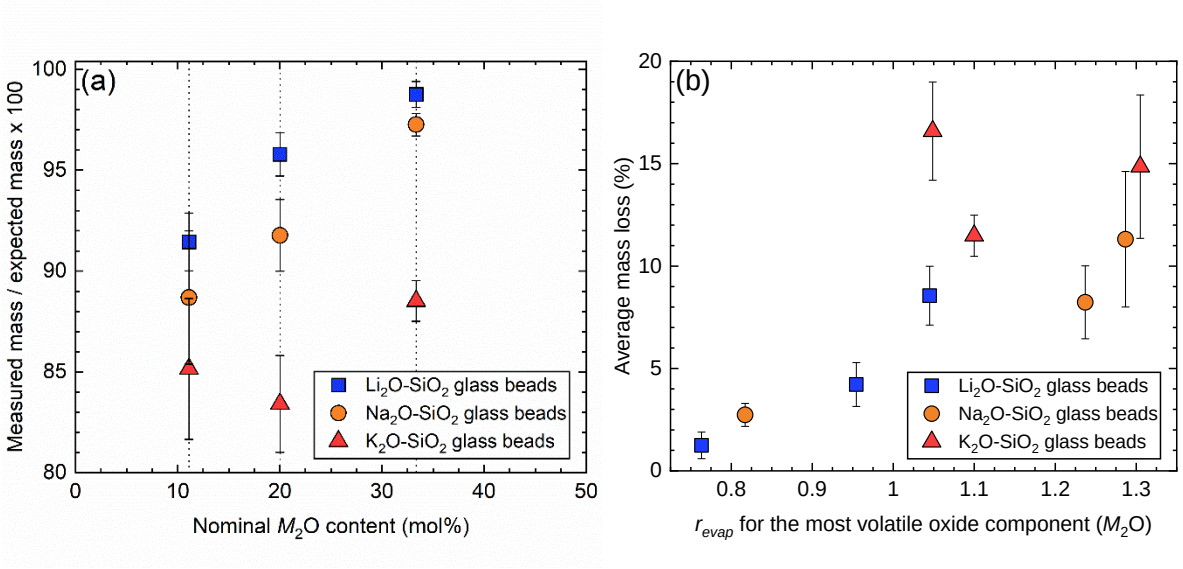

Figure 5. a) Comparison between measured and expected masses of glass beads synthesized by ADL, as a function of their nominal M_2O (M = Li, Na, K) content; error bars correspond to the standard deviation over 10 measured beads. b) correlation between the average mass loss of each target composition and the r_{evap} value of its most volatile component (alkali oxide M_2O).

LA-ICP-MS measurements performed on one representative bead for each composition confirmed these observations (**Fig. 6**): Li_2O-containing beads plotted very close to the 1:1 diagonal, i.e. their measured composition was very close to the nominal one. On the contrary, those containing Na_2O and K_2O were invariably found to plot lower, signaling a non-negligible alkali loss during melting. SiO_2-rich matrices

such as NS8 and KS8 lost up to 80% of their initial alkali oxide content; these losses exhibited a correlation to the values of Δ_{evap} for the respective composition.

All in all, the samples exhibiting the highest mass losses and chemical drifts corresponded to those richer in bubbles (Fig. 4): considering that a better fining could have only been achieved at higher temperatures (i.e. at lower viscosity) or with longer high-temperature dwells (which would have aggravated high-temperature vaporization), it is easy to see that certain compositions are intrinsically unsuitable for the synthesis of glass beads by ADL. This concept is developed and specified in the following.

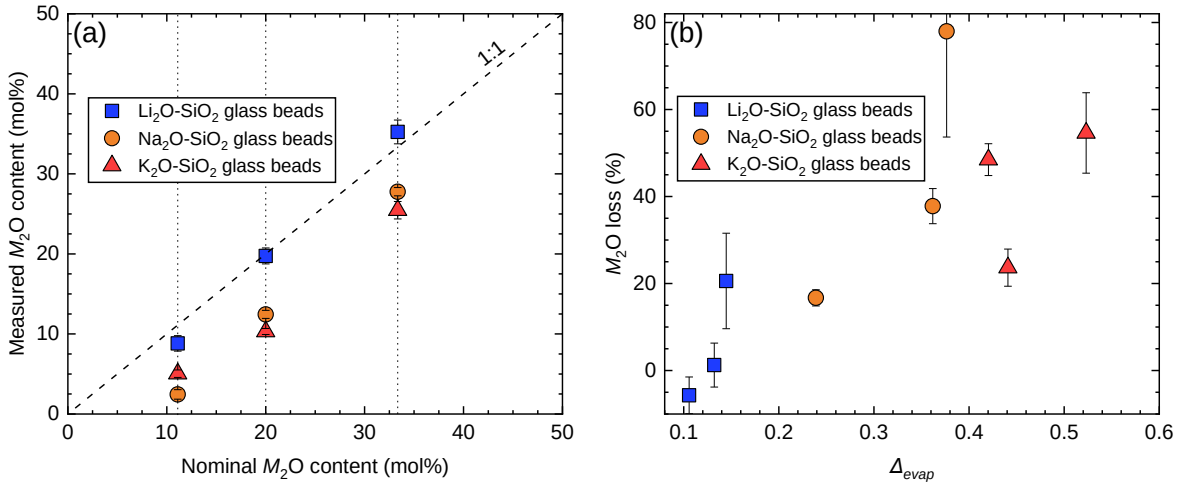

Figure 6. a) Comparison between nominal M_2O content (M = Li, Na, K) of the nine samples synthesized by ADL and the values measured by LA-ICP-MS on representative beads; b) correlation between the M_2O loss in each of the measured beads and the Δ_{evap} value of the respective target composition.

4. Discussion

This simple study highlights some critical aspects of the ADL method for the synthesis of oxide glass beads, with the goal of extending its applicability to broader compositional landscapes, involving for example highly volatile components. From the point of view of mere glass formation, this technique exhibits unrivalled versatility: (i) its containerless conditions suppress heterogeneous nucleation of crystal phases and avoid contamination from crucible and refractory materials; (ii) laser heating can attain up to

~3300 K, above the melting temperature of any stable oxide material; (iii) the setup enables fast cooling rates in the order of several hundreds of K s^{-1} (depending on levitation gas, bead size and composition), facilitating the quenching of melts prone to devitrification. Considering these advantageous features, it would appear that the ADL method should invariably represent the optimal choice for the obtainment of homogeneous, bubble-free beads of a desired stoichiometry. Nevertheless, the results obtained here signal that other key melt properties contribute to determine the suitability of a given composition for ADL synthesis, which can be evaluated beforehand for a smart compositional design.

As known from conventional glass production[75], fining and bubble removal can only be accomplished if the melt viscosity allows for bubble escape[76]. More specifically to ADL synthesis, sufficient melt fluidity is also necessary to form a sufficiently spherical droplet and obtain stable levitation on the gas jet. It is therefore apparent that melt viscosity plays a major role in determining successful ADL synthesis of bubble-free glass beads. An evaluation of viscosity at the melting temperature T_m is thereby particularly revealing, since it represents the lowest temperature at which a liquid droplet can be obtained during heating, minimizing evaporation risks that could affect the sample at higher temperatures. The comparison among some representative glass formers (**Fig. 7**, melting temperatures[69–71, 77–84] and viscosity estimations[61, 63, 81, 85–87] from previous literature) emphasizes how the lowest viscosity possibly obtainable in a stable melt can vary substantially according to composition: while less polymerized or less strongly bonded aluminate and tellurate liquids are immediately very fluid after melting ($\log_{10}\eta(T_m) < 1$), (alumino)silicate melts plot at noticeably higher viscosities. In the case of fully polymerized SiO_2 and GeO_2, $\log_{10}\eta(T_m)$ values exceed 4 and sufficiently low viscosity for bubble removal can only be achieved at very high temperature after substantial mass losses, which could explain the virtually complete absence of literature on the reproducible ADL synthesis of transparent bubble-free beads of these yet very good glass formers.

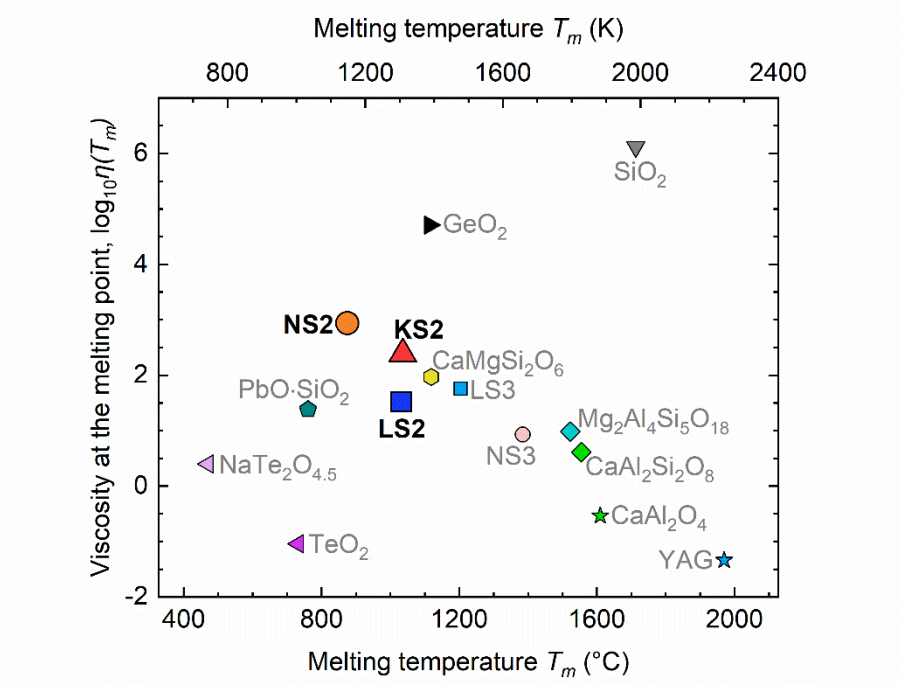

Figure 7. Correlation between melting temperatures T_m and viscosity at T_m $\log_{10}\eta(T_m)$ for a range of representative glass-forming melts, based on viscosity data from this work (LS2, NS2 and KS2) and reliable literature sources (see related text for references).

Obviously, high viscosity at T_m will force the ADL operator to increase laser power until sufficient fluidity can be achieved for homogenization and bubble escape. When dealing with viscous melts ($\log_{10}\eta(T_m) > 1$ on Fig. 7), it is therefore necessary to take into account their susceptibility towards differential high-temperature evaporation of their chemical components (i.e. Δ_{evap}), which could cause compositional drifts. As also supported by the results of this work, alkali oxides are for instance more volatile than SiO_2 and tend to be lost during high temperature melting[88–90], leading to an overall SiO_2 enrichment. Although quantitative estimations of the tendency of simple oxides towards thermal vaporization are available in the literature[48–50], they are difficult to apply to multicomponent systems. Moreover, numerous studies analyzed high-temperature evaporation in melts of geological relevance[91–93], but no overarching understanding of these processes has been offered yet, especially in the case of exotic compositions. Here, the empirical parameters r_{evap} and Δ_{evap} have been shown to predict with satisfactory

reliability the risk of compositional drifts during ADL synthesis, empirically identifying the most sensitive component(s) with an alternative method to the consultation of high-temperature vaporization rates of simple oxides[48–50]. Particularly when the achievement of low viscosity for bubble removal requires heating above the T_m of the target glass by hundreds of kelvins, the results of this work suggest that non-negligible high-temperature evaporation should be expected for r_{evap} values significantly exceeding ~0.8, although this threshold may vary according to the chosen composition, ADL setup, levitation gas, desired final bead size and melting procedure. For instance, a shorter high-temperature dwell may limit vaporization, though possibly preventing satisfactory homogenization and fining. Similarly, Δ_{evap} values above ~0.2 signaled a high risk of compositional drift for the Na_2O- and K_2O-bearing samples synthesized within this work, stressing the general need to minimize this parameter during compositional design. Incidentally, Δ_{evap} minimization can be obtained through the choice of (near-)eutectic compositions, which are also typically known to represent the most favorable regions for glass formation in a phase diagram.

Extending this treatment to other compositions of possible interest for glass scientists (Fig. 8), it is easy to see that r_{evap} values are able to reproduce the comparatively high volatility[48–50] of glass former oxides such as B_2O_3 or TeO_2. As for aluminates such as $CaAl_2O_4$ and $Y_3Al_5O_{12}$, their high melting temperature brings the r_{evap} of their constituting oxides to relatively high values (0.8-1): indeed, previous authors reported non-negligible mass loss from SrO-Al_2O_3 melts during ADL synthesis[94], although no significant compositional drifts should be expected due to the low Δ_{evap} (vertical arrows). Note that the calculation of r_{evap} is expected to estimate less precisely the evaporation behavior of elements prone to oxyreduction such as transition metals, since melting or decomposition temperatures of the respective oxides can strongly depend on the oxidation state.

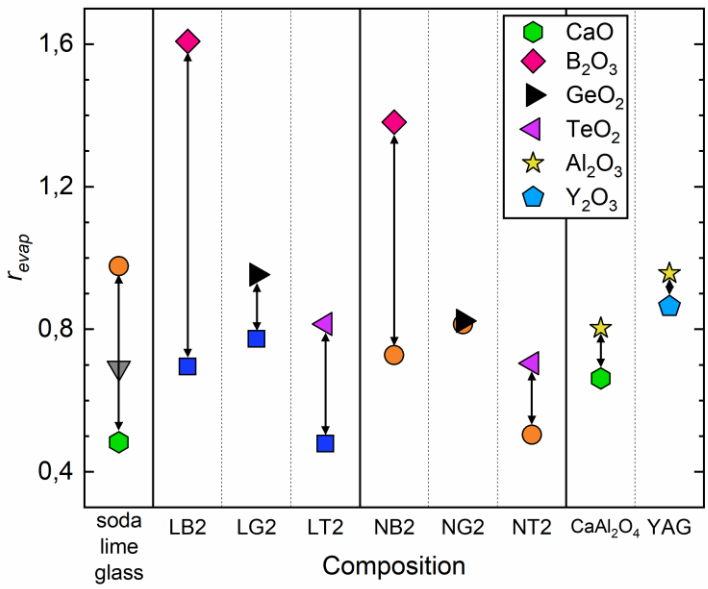

Figure 8. r_{evap} parameters computed for some representative glass-forming substances (LB2: $Li_2O{\cdot}2B_2O_3$, LG2: $Li_2O{\cdot}2GeO_2$, LT2: $Li_2O{\cdot}2TeO_2$, NB2: $Na_2O{\cdot}2B_2O_3$, NG2: $Na_2O{\cdot}2GeO_2$, NT2: $Na_2O{\cdot}2TeO_2$, YAG: $3Y_2O_3{\cdot}5Al_2O_3$); vertical arrows are a graphical representation of Δ_{evap}. Melting temperatures were obtained from previous literature[69–71, 80–82, 95–100]. See also Fig. 3-a for a complete symbol legend.

To finally test the outlined approach and demonstrate the applicability of ADL synthesis to compositions including volatile components, two additional samples were prepared: LB2 ($Li_2O{\cdot}2B_2O_3$) and NP ($Na_2O{\cdot}P_2O_5$), whose key melt properties are summarized in Table 3. Due to their comparatively low melting temperature and low viscosity, both glasses could easily be prepared in the form of bubble-free beads (Fig. 9); their measured composition closely corresponded to the nominal one, ruling out the occurrence of major volatilization during laser heating. Intentional melting of LB2 at higher temperatures (~1200°C on the pyrometer reading) led instead to mass losses up to 45% and to a general enrichment of the melt in B_2O_3, which made evident the merely qualitative character of the estimation of volatilization tendencies using r_{evap} and Δ_{evap}. Although the molar loss in B_2O_3 from the samples was substantially higher than that in Li_2O (Fig. 9-b), the difference was clearly not as pronounced as expectable from the values

plotted in Fig. 8. As such, ADL users approaching the synthesis of a new composition should consider these empirical parameters as a valuable indicative tool, though being aware of their inability to quantitatively capture the subtleties of evaporation mechanism and kinetics.

Table 3. Key melt parameters for samples LB2 and NP: melting temperatures[96, 101, 102] T_m, approximate viscosity[103, 104] at the melting temperature $log_{10}\eta(T_m)$, r_{evap} for the respective oxide components and Δ_{evap}.

Sample	Composition	T_m (K)	$log_{10}\eta(T_m)$ (η in Pa s)	r_{evap} Li_2O	r_{evap} Na_2O	r_{evap} B_2O_3	r_{evap} P_2O_5	Δ_{evap}
LB2	$Li_2O{\cdot}2B_2O_3$	1190	< 0	0.69	-	1.61	-	0.92
NP	$Na_2O{\cdot}P_2O_5$	900	0.3	-	0.64	-	1.06	0.42

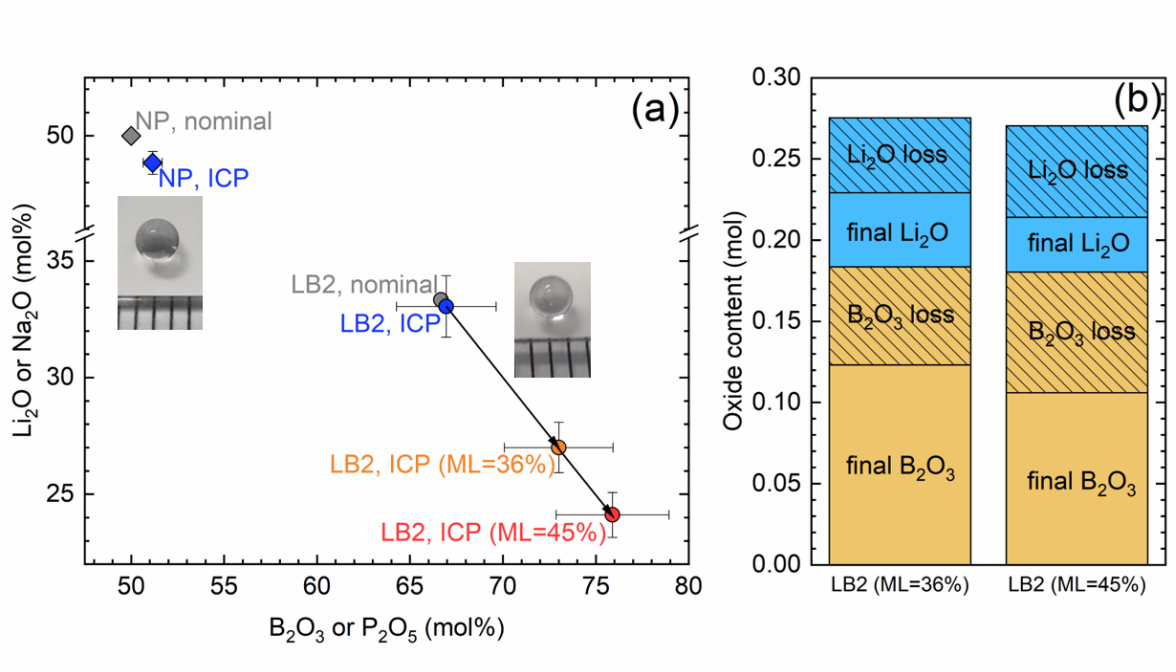

Figure 9. (a) Results of LA-ICP-MS measurements performed on glass beads synthesized by the ADL method for $Na_2O{\cdot}P_2O_5$ (NP) and $Li_2O{\cdot}2B_2O_3$ (LB2) compositions. The data points labelled as "NP, ICP" and "LB2, ICP" correspond to the average of several beads synthesized without evident signs of evaporation (pictures are provided as onsets). In the case of LB2, two beads were intentionally melted at higher

temperatures to induce volatilization, with mass losses (ML) up to 45% of the expected mass. (b) LA-ICP-MS results for the beads that underwent mass losses up to 45%, recalculated in terms of the actual molar Li_2O and B_2O_3 content of the two samples.

5. Conclusions

Aerodynamic levitation coupled to laser heating represents a highly prized method for glass synthesis, new materials discovery and high-temperature in-situ melt characterization. Evaporation of volatile components during laser melting has however noticeably limited its applicability over an extended compositional landscape. This study reveals that the viscosity at the melting temperature $log_{10}\eta(T_m)$ should be critically evaluated before the synthesis: for $log_{10}\eta(T_m) < 1$, glass-forming melts will be easily obtained as bubble-free beads without major volatilization concerns. In case of more viscous melts, the empirical parameters r_{evap} and Δ_{evap} can support a smart compositional design minimizing high-temperature mass loss and chemical drifts.

Acknowledgements

Jan Baborak wishes to acknowledge the Barrande Fellowship Program coordinated by the French Institute in Prague (IFP) and the Czech Ministry of Education, Youth and Sports (MEYS). This work was supported by the specific UCT university research funding, Grant No. A2_FCHT_2022_075. Alessio Zandonà wishes to acknowledge the Deutsche Forschungsgemeinschaft (DFG), project n. 448961237, ZA 1188/1-1 and ZA 1188/2-1. All authors wish to acknowledge Bernard Gratuze from IRAMAT-CEB (UMR7065) for the LA-ICP-MS measurements.

6. References

1. Chopinet M-H. The History of Glass. In: Musgraves JD, Hu J, Calvez L, eds. *Springer Handbook of Glass*. Cham: Springer International Publishing; 2019:1–47. https://doi.org/10.1007/978-3-319-93728-1_1
2. Laniel R, Hubert M, Miroir M, Brient A. Glass Shaping. In: Musgraves JD, Hu J, Calvez L, eds. *Springer Handbook of Glass*. Cham: Springer International Publishing; 2019:1259–1292. https://doi.org/10.1007/978-3-319-93728-1_36
3. Pallaver K. From Venice to East Africa: History, uses, and meanings of glass beads. In: Grewe B-S, Hofmeester K, eds. *Luxury in Global Perspective: Objects and Practices, 1600–2000*. Cambridge: Cambridge University Press; 2016:192–217. https://doi.org/10.1017/9781316257913.008
4. Yuan J, Emura K, Farnham C, Sakai H. Application of glass beads as retro-reflective facades for urban heat island mitigation: Experimental investigation and simulation analysis. *Building and Environment*. 2016;105:140–152. https://doi.org/10.1016/j.buildenv.2016.05.039
5. Searight CE, Alexander EM, Jackson JRR. Method for manufacturing glass beads. US Patent 3,323,888. n.d.
6. Wood TK. Apparatus for manufacturing glass beads. US Patent 2,945,326. n.d.
7. Gruenwald A. Apparatus for forming glass beads and the like articles. US Patent 2,456,697. n.d.
8. Weber JKR. The Containerless Synthesis of Glass. *International Journal of Applied Glass Science*. 2010;1(3):248–256. https://doi.org/10.1111/j.2041-1294.2010.00026.x
9. Nordine PC, Atkins RM. Aerodynamic levitation of laser-heated solids in gas jets. *Review of Scientific Instruments*. 1982;53(9):1456–1464. https://doi.org/10.1063/1.1137196
10. Hennet L, Cristiglio V, Kozaily J, *et al.* Aerodynamic levitation and laser heating: *The European Physical Journal Special Topics*. 2011;196(1):151. https://doi.org/10.1140/epjst/e2011-01425-0
11. Winborne DA, Nordine PC, Rosner DE, Marley NF. Aerodynamic levitation technique for containerless high temperature studies on liquid and solid samples. *Metallurgical Transactions B*. 1976;7(4):711–713. https://doi.org/10.1007/BF02698607
12. Oganov AR, Pickard CJ, Zhu Q, Needs RJ. Structure prediction drives materials discovery. *Nature Reviews Materials*. 2019;4(5):331–348. https://doi.org/10.1038/s41578-019-0101-8
13. Skinner LB, Barnes AC, Crichton W. Novel behaviour and structure of new glasses of the type Ba–Al–O and Ba–Al–Ti–O produced by aerodynamic levitation and laser heating. *Journal of Physics: Condensed Matter*. 2006;18(32):L407–L414. https://doi.org/10.1088/0953-8984/18/32/l01
14. Xu C, Wang C, Yu J, *et al.* Structure and optical properties of Er-doped CaO-Al2O3 (Ga2O3) glasses fabricated by aerodynamic levitation. *Journal of the American Ceramic Society*. 2017;100(7):2852–2858. https://doi.org/10.1111/jace.14862
15. Zhang X, Zhang M, Zhang J, Li Y, Gu Y, Qi X. Photoluminescence, transmittance and electrical properties of Eu3+-doped Al2O3-SrO glasses synthesized by an aerodynamic levitation technique. *Journal of Luminescence*. 2019;206:79–83. https://doi.org/10.1016/j.jlumin.2018.10.040
16. Castaing V, Monteiro C, Sontakke AD, *et al.* Hexagonal Sr1−x/2Al2−xSixO4:Eu2+,Dy3+ transparent ceramics with tuneable persistent luminescence properties. *Dalton Trans*. 2020;49(46):16849–16859. https://doi.org/10.1039/D0DT03137B
17. Fernandez-Carrion AJ, Al Saghir K, Veron E, *et al.* Local Disorder and Tunable Luminescence in Sr1–x/2Al2–xSixO4 (0.2 ≤ x ≤ 0.5) Transparent Ceramics. *Inorg Chem*. 2017;56(23):14446–14458. https://doi.org/10.1021/acs.inorgchem.7b01881
18. Alahraché S, Deschamps M, Lambert J, *et al.* Crystallization of Y2O3–Al2O3 Rich Glasses: Synthesis of YAG Glass-Ceramics. *J Phys Chem C*. 2011;115(42):20499–20506. https://doi.org/10.1021/jp207516w

19. Alahraché S, Al Saghir K, Chenu S, *et al.* Perfectly Transparent Sr3Al2O6 Polycrystalline Ceramic Elaborated from Glass Crystallization. *Chem Mater*. 2013;25(20):4017–4024. https://doi.org/10.1021/cm401953d
20. Rosales-Sosa GA, Masuno A, Higo Y, *et al.* High Elastic Moduli of a 54Al2O3-46Ta2O5 Glass Fabricated via Containerless Processing. *Scientific Reports*. 2015;5(1):15233. https://doi.org/10.1038/srep15233
21. Yoshimoto K, Masuno A, Ueda M, Inoue H, Yamamoto H, Kawashima T. Low phonon energies and wideband optical windows of La2O3-Ga2O3 glasses prepared using an aerodynamic levitation technique. *Scientific Reports*. 2017;7(1):45600. https://doi.org/10.1038/srep45600
22. Yoshimoto K, Ezura Y, Ueda M, Masuno A, Inoue H. 2.7 μm Mid-Infrared Emission in Highly Erbium-Doped Lanthanum Gallate Glasses Prepared Via an Aerodynamic Levitation Technique. *Advanced Optical Materials*. 2018;6(8):1701283. https://doi.org/10.1002/adom.201701283
23. Calzavara F, Allix M, Dussauze M, *et al.* Glass forming regions, structure and properties of lanthanum barium germanate and gallate glasses. *Journal of Non-Crystalline Solids*. 2021;571:121064. https://doi.org/10.1016/j.jnoncrysol.2021.121064
24. Bazzaoui H, Genevois C, Massiot D, *et al.* Stabilization of the Trigonal Langasite Structure in Ca3Ga2–2xZnxGe4+xO14 (0 ≤ x ≤ 1) with Partial Ordering of Three Isoelectronic Cations Characterized by a Multitechnique Approach. *Inorg Chem*. 2022;61(24):9339–9351. https://doi.org/10.1021/acs.inorgchem.2c01173
25. Xiang H, Guan L, Peng Z, Li J. Preparation of high refractive index La2O3–TiO2 glass by aerodynamic levitation technique and effects of Bi2O3 substitution on its thermal and optical properties. *Ceramics International*. 2014;40(3):4985–4988. https://doi.org/10.1016/j.ceramint.2013.10.014
26. Zhang M, Wen H, Pan X, *et al.* Study on novel high refractive index La2O3-Lu2O3-TiO2 glasses prepared by aerodynamic levitation method. *Materials Letters*. 2018;222:5–7. https://doi.org/10.1016/j.matlet.2018.03.120
27. Ma X, Peng Z, Li J. Effect of Ta2O5 Substituting on Thermal and Optical Properties of High Refractive Index La2O3–Nb2O5 Glass System Prepared by Aerodynamic Levitation Method. *Journal of the American Ceramic Society*. 2015;98(3):770–773. https://doi.org/10.1111/jace.13384
28. Li J, Li J, Li B, Yu J, Qi L. An Upconversion Niobium Pentoxide Bulk Glass Codoped with Er3+/Yb3+ Fabricated by Aerodynamic Levitation Method. *Journal of the American Ceramic Society*. 2015;98(6):1865–1869. https://doi.org/10.1111/jace.13551
29. Yoshimoto K, Masuno A, Inoue H, Watanabe Y. Transparent and High Refractive Index La2O3–WO3 Glass Prepared Using Containerless Processing. *Journal of the American Ceramic Society*. 2012;95(11):3501–3504. https://doi.org/10.1111/j.1551-2916.2012.05439.x
30. Pack A, Kremer K, Albrecht N, Simon K, Kronz A. Description of an aerodynamic levitation apparatus with applications in Earth sciences. *Geochemical Transactions*. 2010;11(1):4. https://doi.org/10.1186/1467-4866-11-4
31. Alderman OLG, Wilding MC, Tamalonis A, *et al.* Iron K-edge X-ray absorption near-edge structure spectroscopy of aerodynamically levitated silicate melts and glasses. *Chemical Geology*. 2017;453:169–185. https://doi.org/10.1016/j.chemgeo.2017.01.020
32. Gueguen Y, Houizot P, Célarié F, *et al.* Structure and viscosity of phase-separated BaO–SiO2 glasses. *Journal of the American Ceramic Society*. 2017;100(5):1982–1993. https://doi.org/10.1111/jace.14642
33. Martel L, Allix M, Millot F, *et al.* Controlling the Size of Nanodomains in Calcium Aluminosilicate Glasses. *J Phys Chem C*. 2011;115(39):18935–18945. https://doi.org/10.1021/jp200824m
34. Skinner LB, Benmore CJ, Weber JKR, Wilding MC, Tumber SK, Parise JB. A time resolved high energy X-ray diffraction study of cooling liquid SiO2. *Phys Chem Chem Phys*. 2013;15(22):8566–8572. https://doi.org/10.1039/C3CP44347G

35. Kulik E, Nishiyama N, Masuno A, *et al.* A Complete Solid Solution with Rutile-Type Structure in SiO2–GeO2 System at 12 GPa and 1600°C. *Journal of the American Ceramic Society*. 2015;98(12):4111–4116. https://doi.org/10.1111/jace.13859
36. Nasikas NK, Edwards TG, Sen S, Papatheodorou GN. Structural Characteristics of Novel Ca–Mg Orthosilicate and Suborthosilicate Glasses: Results from 29Si and 17O NMR Spectroscopy. *J Phys Chem B*. 2012;116(9):2696–2702. https://doi.org/10.1021/jp212469p
37. Skinner LB, Benmore CJ, Weber JKR, *et al.* Structure of Molten CaSiO3: Neutron Diffraction Isotope Substitution with Aerodynamic Levitation and Molecular Dynamics Study. *J Phys Chem B*. 2012;116(45):13439–13447. https://doi.org/10.1021/jp3066019
38. Suzuki F, Sato F, Oshita H, Yao S, Nakatsuka Y, Tanaka K. Large Faraday effect of borate glasses with high Tb3+ content prepared by containerless processing. *Optical Materials*. 2018;76:174–177. https://doi.org/10.1016/j.optmat.2017.12.031
39. Alderman OLG, Liška M, Macháček J, *et al.* Temperature-Driven Structural Transitions in Molten Sodium Borates Na2O–B2O3: X-ray Diffraction, Thermodynamic Modeling, and Implications for Topological Constraint Theory. *J Phys Chem C*. 2016;120(1):553–560. https://doi.org/10.1021/acs.jpcc.5b10277
40. Alderman OLG, Benmore CJ, Reynolds B, Royle B, Feller S, Weber RJK. Liquid fragility maximum in lithium borate glass-forming melts related to the local structure. *International Journal of Applied Glass Science*. 2023;14(1):52–68. https://doi.org/10.1111/ijag.16611
41. M. C. Wilding, C. J. Benmore, J. A. Tangeman, S. Sampath. Coordination changes in magnesium silicate glasses. *Europhysics Letters*. 2004;67(2):212. https://doi.org/10.1209/epl/i2003-10286-8
42. SAITO Y, YONEMURA T, MASUNO A, INOUE H, OHARA K, KOHARA S. Structural change of Na2O-doped SiO2 glasses by melting. *Journal of the Ceramic Society of Japan*. 2016;124(6):717–720. https://doi.org/10.2109/jcersj2.16028
43. Kohara S, Suzuya K, Takeuchi K, *et al.* Glass Formation at the Limit of Insufficient Network Formers. *Science*. 2004;303(5664):1649–1652. https://doi.org/10.1126/science.1095047
44. Lelong G, Cormier L, Hennet L, *et al.* Lithium Borates from the Glass to the Melt: A Temperature-Induced Structural Transformation Viewed from the Boron and Oxygen Atoms. *Inorg Chem*. 2021;60(2):798–806. https://doi.org/10.1021/acs.inorgchem.0c02844
45. SASAKI S, MASUNO A. Composition dependence of the local structure and transparency of Gd2O3–B2O3 binary glasses prepared via aerodynamic levitation. *Journal of the Ceramic Society of Japan*. 2022;130(1):60–64. https://doi.org/10.2109/jcersj2.21124
46. Zandonà A, Castaing V, Shames AI, *et al.* Oxidation and coordination states assumed by transition metal dopants in an invert ultrabasic silicate glass. *Journal of Non-Crystalline Solids*. 2023;603:122094. https://doi.org/10.1016/j.jnoncrysol.2022.122094
47. Bazzaoui H, Genevois C, Véron E, Pitcher MJ, Allix M, Zandonà A. Towards new zero-thermal-expansion materials: Li-free quartz solid solutions stuffed with transition metal cations. *Journal of the European Ceramic Society*. 2022. https://doi.org/10.1016/j.jeurceramsoc.2022.11.035
48. Brewer Leo. Thermodynamic Properties of the Oxides and their Vaporization Processes. *Chem Rev*. 1953;52(1):1–75. https://doi.org/10.1021/cr60161a001
49. Lamoreaux RH, Hildenbrand DL, Brewer L. High-Temperature Vaporization Behavior of Oxides II. Oxides of Be, Mg, Ca, Sr, Ba, B, Al, Ga, In, Tl, Si, Ge, Sn, Pb, Zn, Cd, and Hg. *Journal of Physical and Chemical Reference Data*. 1987;16(3):419–443. https://doi.org/10.1063/1.555799
50. Lamoreaux RH, Hildenbrand DL. High Temperature Vaporization Behavior of Oxides. I. Alkali Metal Binary Oxides. *Journal of Physical and Chemical Reference Data*. 1984;13(1):151–173. https://doi.org/10.1063/1.555706

51. Zandonà A, Moustrous M, Genevois C, Véron E, Canizarès A, Allix M. Glass-forming ability and ZrO2 saturation limits in the magnesium aluminosilicate system. *Ceramics International*. 2021. https://doi.org/10.1016/j.ceramint.2021.12.051
52. Zandonà A, Ory S, Genevois C, *et al.* Glass formation and devitrification behavior of alkali (Li, Na) aluminosilicate melts containing TiO2. *Journal of Non-Crystalline Solids*. 2022;582:121448. https://doi.org/10.1016/j.jnoncrysol.2022.121448
53. Zandonà A, Chesneau E, Helsch G, *et al.* Glass-forming ability and structural features of melt-quenched and gel-derived SiO2-TiO2 glasses. *Journal of Non-Crystalline Solids*. 2022;598:121967. https://doi.org/10.1016/j.jnoncrysol.2022.121967
54. Völkel R, Eisner M, Weible KJ. Miniaturized imaging systems. *Microelectronic Engineering*. 2003;67–68:461–472. https://doi.org/10.1016/S0167-9317(03)00102-3
55. Liu X, Wang Y, Yu L, *et al.* Thermal degradation and stability of starch under different processing conditions. *Starch - Stärke*. 2013;65(1–2):48–60. https://doi.org/10.1002/star.201200198
56. Young ED, Macris CA, Tang H, Hogan AA, Shollenberger QR. Isotope velocimetry: Experimental and theoretical demonstration of the potential importance of gas flow for isotope fractionation during evaporation of protoplanetary material. *Earth and Planetary Science Letters*. 2022;589:117575. https://doi.org/10.1016/j.epsl.2022.117575
57. Press WH, Teukolsky SA. Savitzky-Golay Smoothing Filters. *Computers in Physics*. 1990;4(6):669–672. https://doi.org/10.1063/1.4822961
58. Hrubý A. Evaluation of glass-forming tendency by means of DTA. *Czechoslovak Journal of Physics B*. 1972;22(11):1187–1193. https://doi.org/10.1007/BF01690134
59. Scherer GW. Use of the Adam-Gibbs Equation in the Analysis of Structural Relaxation. *Journal of the American Ceramic Society*. 1984;67(7):504–511. https://doi.org/10.1111/j.1151-2916.1984.tb19643.x
60. Yue Y, von der Ohe R, Jensen SL. Fictive temperature, cooling rate, and viscosity of glasses. *J Chem Phys*. 2004;120(17):8053–8059. https://doi.org/10.1063/1.1689951
61. Al-Mukadam R, Di Genova D, Bornhöft H, Deubener J. High rate calorimetry derived viscosity of oxide melts prone to crystallization. *Journal of Non-Crystalline Solids*. 2020;536:119992. https://doi.org/10.1016/j.jnoncrysol.2020.119992
62. Di Genova D, Zandona A, Deubener J. Unravelling the effect of nano-heterogeneity on the viscosity of silicate melts: Implications for glass manufacturing and volcanic eruptions. *Journal of Non-Crystalline Solids*. 2020;545:120248. https://doi.org/10.1016/j.jnoncrysol.2020.120248
63. Al-Mukadam R, Zandona A, Deubener J. Kinetic fragility of pure TeO2 glass. *Journal of Non-Crystalline Solids*. 2021;554:120595. https://doi.org/10.1016/j.jnoncrysol.2020.120595
64. Shartsis L, Spinner S, Capps W. Density, Expansivity, and Viscosity of Molten Alkali Silicates. *Journal of the American Ceramic Society*. 1952;35(6):155–160. https://doi.org/10.1111/j.1151-2916.1952.tb13090.x
65. Mauro JC, Yue Y, Ellison AJ, Gupta PK, Allan DC. Viscosity of glass-forming liquids. *Proceedings of the National Academy of Sciences*. 2009;106(47):19780–19784. https://doi.org/10.1073/pnas.0911705106
66. Waterton S. The viscosity-temperature relationship and some inferences on the nature of molten and of plastic glass. *J Soc Glass Technol*. 1932;16:244–247.
67. Gratuze B. Glass Characterization Using Laser Ablation-Inductively Coupled Plasma-Mass Spectrometry Methods. In: Dussubieux L, Golitko M, Gratuze B, eds. *Recent Advances in Laser Ablation ICP-MS for Archaeology*. Berlin, Heidelberg: Springer; 2016:179–196. https://doi.org/10.1007/978-3-662-49894-1_12

68. Nascimento MLF, Souza LA, Ferreira EB, Zanotto ED. Can glass stability parameters infer glass forming ability? *Journal of Non-Crystalline Solids*. 2005;351(40):3296–3308. https://doi.org/10.1016/j.jnoncrysol.2005.08.013
69. Kracek FC. The Binary System Li2O–SiO2. *J Phys Chem*. 1930;34(12):2641–2650. https://doi.org/10.1021/j150318a001
70. Kim SS, Sanders Jr. TH. Thermodynamic Modeling of Phase Diagrams in Binary Alkali Silicate Systems. *Journal of the American Ceramic Society*. 1991;74(8):1833–1840. https://doi.org/10.1111/j.1151-2916.1991.tb07796.x
71. Blander M, Pelton AD. Thermodynamic analysis of binary liquid silicates and prediction of ternary solution properties by modified quasichemical equations. *Geochimica et Cosmochimica Acta*. 1987;51(1):85–95. https://doi.org/10.1016/0016-7037(87)90009-3
72. Annamalai P, Shankar N, Cole R, Subramanian RS. Bubble migration inside a liquid drop in a space laboratory. *Applied Scientific Research*. 1982;38(1):179–186. https://doi.org/10.1007/BF00385947
73. Brone D, Cole R. Bubble trajectories in rotating drops. *Advances in Space Research*. 1991;11(7):243–246. https://doi.org/10.1016/0273-1177(91)90290-Z
74. Ruggles JS, Cook RG, Cole R. Microgravity bubble migration in rotating flows. *Journal of Spacecraft and Rockets*. 1990;27(1):43–47. https://doi.org/10.2514/3.26103
75. Hubert M. Industrial Glass Processing and Fabrication. In: Musgraves JD, Hu J, Calvez L, eds. *Springer Handbook of Glass*. Cham: Springer International Publishing; 2019:1195–1231. https://doi.org/10.1007/978-3-319-93728-1_34
76. JUCHA RB, POWERS D, McNEIL T, SUBRAMANIAN RS, COLE R. Bubble Rise in Glassmelts. *Journal of the American Ceramic Society*. 1982;65(6):289–292. https://doi.org/10.1111/j.1151-2916.1982.tb10446.x
77. RICKER RW, OSBORN EF. Additional Phase Equilibrium Data for the System CaO-MgO-SiO2. *Journal of the American Ceramic Society*. 1954;37(3):133–139. https://doi.org/10.1111/j.1151-2916.1954.tb14011.x
78. Kamiya K, Yoko T, Hashimoto Y, Sakka S. Crystallization behavior of xNa2O· (1−x)GeO2 glasses and melts with x of 0 to 0.30. *Materials Research Bulletin*. 1988;23(3):363–369. https://doi.org/10.1016/0025-5408(88)90010-4
79. SMART RM, GLASSER FP. Compound Formation and Phase Equilibria in the System PbO-SiO2. *Journal of the American Ceramic Society*. 1974;57(9):378–382. https://doi.org/10.1111/j.1151-2916.1974.tb11416.x
80. Kavaklıoğlu KB, Aydin S, Çelikbilek M, Ersundu AE. The TeO2-Na2O System: Thermal Behavior, Structural Properties, and Phase Equilibria. *International Journal of Applied Glass Science*. 2015;6(4):406–418. https://doi.org/10.1111/ijag.12103
81. Fratello VJ, Brandle CD. Physical properties of a Y3Al5012 melt. *Journal of Crystal Growth*. 1993;128(1, Part 2):1006–1010. https://doi.org/10.1016/S0022-0248(07)80087-X
82. Chatterjee AK, Zhmoidin GI. The phase equilibrium diagram of the system CaO-Al2O3-CaF2. *Journal of Materials Science*. 1972;7(1):93–97. https://doi.org/10.1007/BF00549555
83. Eriksson G, Pelton AD. Critical evaluation and optimization of the thermodynamic properties and phase diagrams of the CaO-Al2O3, Al2O3-SiO2, and CaO-Al2O3-SiO2 systems. *Metallurgical Transactions B*. 1993;24(5):807–816. https://doi.org/10.1007/BF02663141
84. Schreyer W, Schairer JF. Metastable solid solutions with quartz-type structures on the join SiO2–MgAl2O4. *Zeitschrift für Kristallographie - Crystalline Materials*. 1961;116(1–2):60–82. https://doi.org/10.1524/zkri.1961.116.1-2.60
85. Nascimento MLF, Dutra Zanotto E. Does viscosity describe the kinetic barrier for crystal growth from the liquidus to the glass transition? *J Chem Phys*. 2010;133(17):174701. https://doi.org/10.1063/1.3490793

86. Cassetta M, Di Genova D, Zanatta M, *et al.* Estimating the viscosity of volcanic melts from the vibrational properties of their parental glasses. *Scientific Reports*. 2021;11(1):13072. https://doi.org/10.1038/s41598-021-92407-5
87. Urbain G. Viscosité de liquides du système CaO-Al2O3. *Rev Int Hautes Tempér Réfract Fr*. 1983;20:135–139.
88. Piacente V, Matoušek J. Alkali vapor pressures over some simple silicate melts. *Collect Czech Chem Commun*. 1983;48:1528–1531. https://doi.org/10.1135/cccc19831528
89. Beerkens RGC. Modeling the Kinetics of Volatilization from Glass Melts. *Journal of the American Ceramic Society*. 2001;84(9):1952–1960. https://doi.org/10.1111/j.1151-2916.2001.tb00942.x
90. CHARLES RJ. Activities in Li2O-, Na2O, and K2O-SiO2 Solutions. *Journal of the American Ceramic Society*. 1967;50(12):631–641. https://doi.org/10.1111/j.1151-2916.1967.tb15018.x
91. Sossi PA, Klemme S, O'Neill HStC, Berndt J, Moynier F. Evaporation of moderately volatile elements from silicate melts: experiments and theory. *Geochimica et Cosmochimica Acta*. 2019;260:204–231. https://doi.org/10.1016/j.gca.2019.06.021
92. Badro J, Sossi PA, Deng Z, Borensztajn S, Wehr N, Ryerson FJ. Experimental investigation of elemental and isotopic evaporation processes by laser heating in an aerodynamic levitation furnace. *Comptes Rendus Geoscience*. 2021;353(1):101–114.
93. Mendybaev RA, Richter FM, Georg RB, *et al.* Experimental evaporation of Mg- and Si-rich melts: Implications for the origin and evolution of FUN CAIs. *Geochimica et Cosmochimica Acta*. 2013;123:368–384. https://doi.org/10.1016/j.gca.2013.06.044
94. Shan Z, Liu S, Tao H, Yue Y. Mixed alkaline-earth effects on several mechanical and thermophysical properties of aluminate glasses and melts. *Journal of the American Ceramic Society*. 2019;102(3):1128–1136. https://doi.org/10.1111/jace.15975
95. Zhang Z, Xiao Y, Voncken J, *et al.* Phase Equilibria in the Na2O–CaO–SiO2 System. *Journal of the American Ceramic Society*. 2011;94(9):3088–3093. https://doi.org/10.1111/j.1551-2916.2011.04442.x
96. Yu H, Jin Z, Chen Q, Hillert M. Thermodynamic Assessment of the Lithium-Borate System. *Journal of the American Ceramic Society*. 2000;83(12):3082–3088. https://doi.org/10.1111/j.1151-2916.2000.tb01686.x
97. Meshalkin AB, Kaplun AB, Kidyarov BI. The influence of the compounds dissociation in melting point on melt supercooling. *Journal of Crystal Growth*. 2008;310(7):1362–1365. https://doi.org/10.1016/j.jcrysgro.2007.11.195
98. MURTHY MK, AGUAYO J. Studies in Germanium Oxide Systems: II, Phase Equilibria in the System Na2O—GeO2. *Journal of the American Ceramic Society*. 1964;47(9):444–447. https://doi.org/10.1111/j.1151-2916.1964.tb14433.x
99. MURTHY MK, IP J. Studies in Germanium Oxide Systems: I, Phase Equilibria in the System Li2O—GeO2. *Journal of the American Ceramic Society*. 1964;47(7):328–331. https://doi.org/10.1111/j.1151-2916.1964.tb12995.x
100. Safonov VV, Kravchenko VV, Filatkina NV, Bryksina-Lyamina MM, Chaban NG. *Zh Neorg Khim*. 1989;34(11):2920–2923.
101. Cormia RL, Mackenzie JD, Turnbull D. Viscous Flow and Melt Allotropy of Phosphorus Pentoxide. *Journal of Applied Physics*. 1963;34(8):2245–2248. https://doi.org/10.1063/1.1702721
102. Kropiwnicka J. Phase equilibria in the system La2O3-Na2O-P2O5: Binary phase diagram La(PO3)3-NaPO3. *Journal of thermal analysis*. 1988;34(5):1405–1412. https://doi.org/10.1007/BF01914364
103. Muñoz-Senovilla L, Muñoz F. Behaviour of viscosity in metaphosphate glasses. *Journal of Non-Crystalline Solids*. 2014;385:9–16. https://doi.org/10.1016/j.jnoncrysol.2013.10.021

104. Shartsis L, Spinner S, Capps W. Density, Expansivity, and Viscosity of Molten Alkali Silicates. *Journal of the American Ceramic Society*. 1952;35(6):155–160. https://doi.org/10.1111/j.1151-2916.1952.tb13090.x